ACS APPLIED ENERGY MATERIALS

Editors' Choice

www.acsaem.org

Article

Dense and Uniform Integration of Cu-BDC Particles on a Nafion Film for a High-Performance Hydrogen-Producing Device

Zhijia Xiao, Jinlong Wang, Xinyi Ke, Zihan Lu, Zhe Zhao,* Yongfeng Mei, and Gaoshan Huang*

Cite This: *ACS Appl. Energy Mater.* 2024, 7, 3406−3413

Read Online

ACCESS | Metrics & More | Article Recommendations | Supporting Information

ABSTRACT: The incorporation of metal−organic frameworks onto conductive substrates demonstrates considerable potential in applications related to the hydrogen evolution reaction. In this work, we present a streamlined synthesis approach involving atomic layer deposition pretreatment to facilitate the controlled growth of Cu-BDC particles on a conductive Nafion film. This methodology preserves a substantial loading of Cu-BDC with a hierarchically porous structure, accompanied by a notable surface area of 547 m^2 g^{-1}. The composite is subsequently utilized as an electrocatalyst for hydrogen generation in an alkane electrolyte. The structural advances in the composite result in a superior electrochemical hydrogen production efficiency with a low overpotential of 84 mV and a low Tafel slope of 58 mV dec^{-1} in 1.0 M NaOH. Notably, the composite showed good cycling performance during the 18 h test with 2000 cycles. This research introduces a design of a catalyst electrode with promising implications for the hydrogen production industry.

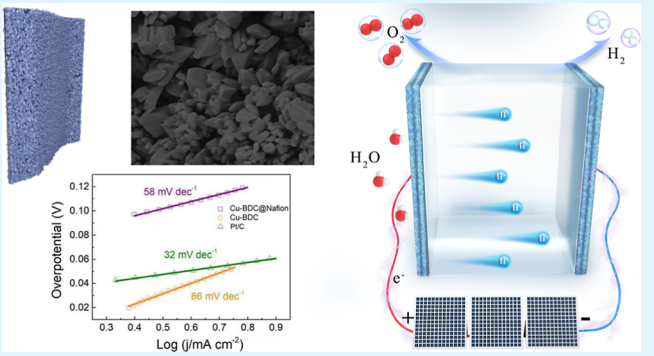

KEYWORDS: *metal−organic frameworks, atomic layer deposition, hierarchical porosity, electrocatalyst, hydrogen evolution reaction*

1. INTRODUCTION

In response to the pressing need to address the energy crisis and the severity of environmental issues, researchers have been actively engaged in the investigation of clean and sustainable energy resources that can substitute conventional fossil fuels.[1,2] Owing to its zero carbon emissions and considerable energy density, hydrogen is universally acknowledged as a promising new energy source poised to accommodate the escalating demand for energy.[3] Several existing methods for hydrogen production, such as coal gasification, steam reforming, and water electrolysis, have been employed.[4] However, the utilization of electrocatalysts to stimulate the hydrogen evolution reaction (HER) has been identified as a particularly efficient methodology for prospective hydrogen production, primarily because of its low reaction environment requirement (room temperature), environmentally friendly hydrogen source (i.e., water), and easy separation of the products (hydrogen and oxygen are produced at different electrodes).[4,5] Electrocatalysts that exhibit high activity and low HER overpotential are crucial for enhancing the sluggish HER kinetics.[6] Up to this point, the Pt-group precious metals have been identified as the most efficient HER electrocatalysts, demonstrating negligible overpotential in acidic solutions.[7,8] Nevertheless, their scarcity and high cost pose significant limitations on their widespread commercial application. Consequently, the search for alternative, low-cost catalysts is an ongoing area of research, with numerous materials possessing a large surface area,[9] high active sites,[10,11] and nonprecious transition metals doped[12−14] having been undertaken in this pursuit.

Metal−organic frameworks (MOFs) are three-dimensional crystals characterized by long-range ordering and composed of transition-metal clusters and corresponding organic frameworks.[15] MOFs are recognized as suitable precursor materials for a myriad of applications in biosensing, catalysis, gas separation, and drug-carrying owing to their favorable attributes, including remarkably high specific surface areas, abundant porosity, and exceptional thermal stability.[16−18] Within the realm of MOFs, Cu-BDC stands out as a significant subclass as they have abundant unsaturated Cu metal sites, which can provide highly catalytic Cu ions for favorable electrochemical applications.[19,20]

However, the poor conductivity of Cu-BDC limits its performance toward HER.[21] In addition, it is challenging to establish a conductive pathway for rapid ion diffusion among dispersed particles.[22] Combining a conductive substrate with Cu-BDC particles has been a good choice to enhance the HER

Received: January 22, 2024
Revised: March 26, 2024
Accepted: March 26, 2024
Published: April 9, 2024

https://doi.org/10.1021/acsaem.4c00170
ACS Appl. Energy Mater. 2024, 7, 3406−3413

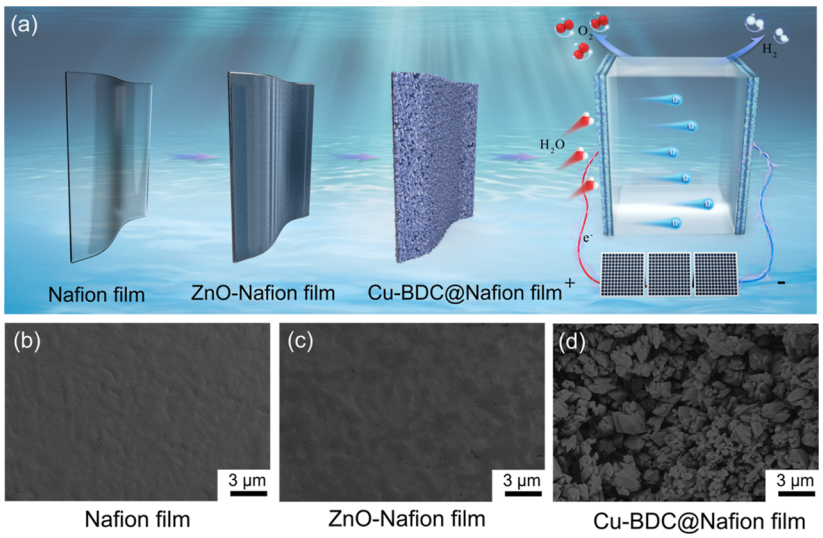

Figure 1. (a) Schematic of the preparation process of the Cu-BDC@Nafion film. SEM images of the (b) Nafion film, (c) ZnO-Nafion film, and (d) Cu-BDC@Nafion film.

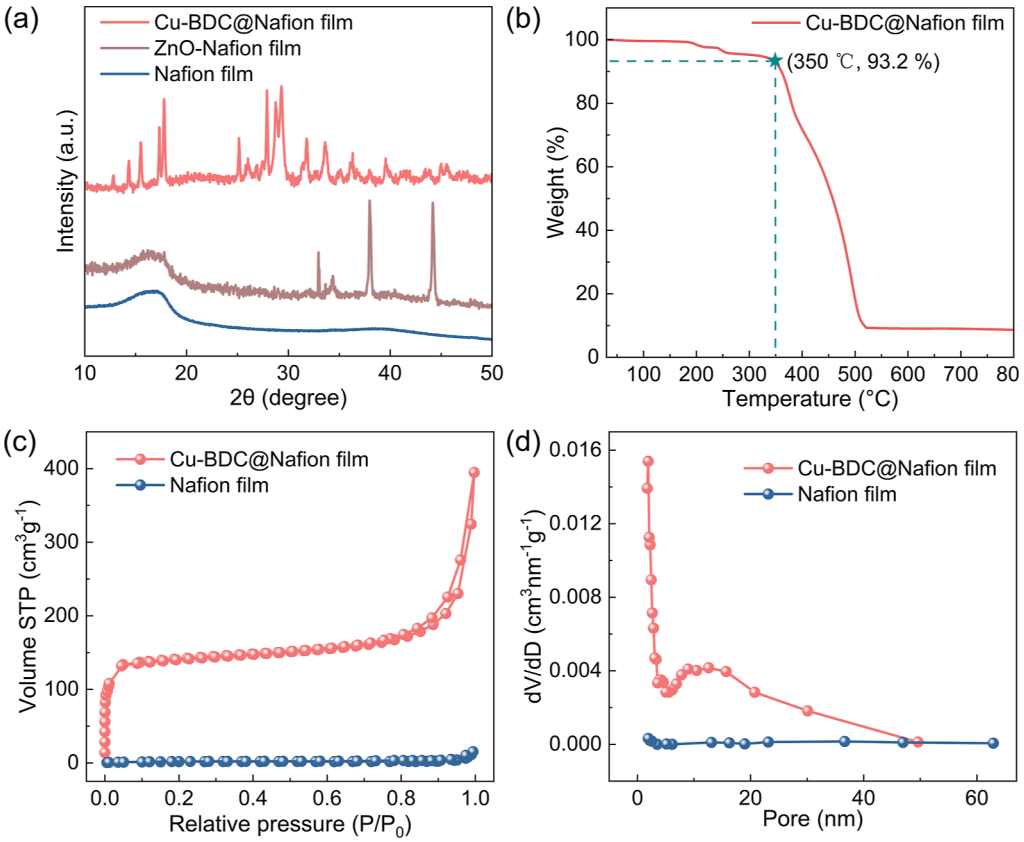

Figure 2. (a) XRD patterns of the Cu-BDC@Nafion film, ZnO-Nafion film, and original Nafion film. (b) TGA curve of the Cu-BDC@Nafion film. (c) Nitrogen adsorption−desorption isotherms of the Cu-BDC@Nafion film and blank Nafion film. (d) Calculated pore size distribution of the Cu-BDC@Nafion film and blank Nafion film.

property.[23] Recently, we have developed an effective strategy for integrating MOFs onto specific substrates, aided by oxide nanomembranes fabricated through atomic layer deposition (ALD).[24,25] Due to the advantages of the high uniformity, high controllability, and good conformality of the ALD approach, MOF films can be prepared on complex substrates with firm adhesion.[26]

Herein, we introduce a fabrication methodology to efficiently synthesize dense Cu-BDC on a conductive Nafion film (Cu-BDC@Nafion film) by utilizing ALD pretreatment. This strategy creates an assembly of Cu-BDC crystals on the Nafion film, resulting in a hierarchically porous film. This Cu-BDC@Nafion film boasts an impressive surface area of 547 m^2 g^{-1}, significantly augmenting the composite's electrocatalytic efficiency. In an alkaline electrolyte, the Cu-BDC@Nafion film

https://doi.org/10.1021/acsaem.4c00170
ACS Appl. Energy Mater. 2024, 7, 3406−3413

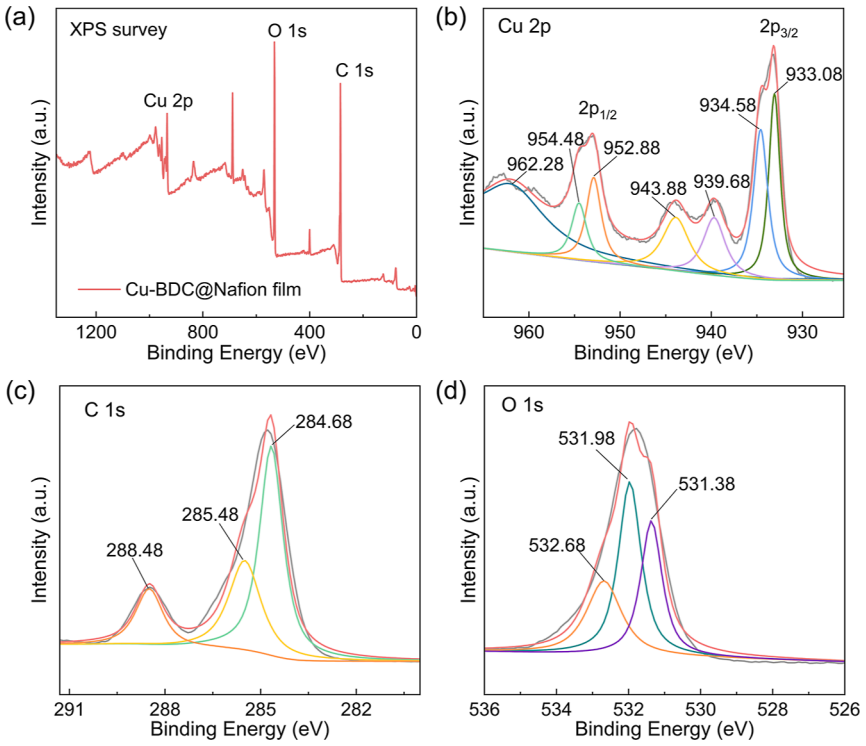

Figure 3. (a) XPS survey scan of the Cu-BDC@Nafion film. High-resolution XPS spectra of (b) Cu 2p, (c) C 1s, and (d) O 1s.

exhibits a very low overpotential of 84 mV to attain the current density of 10 mA cm^{-2} and a low Tafel slope of 58 mV dec^{-1}. Here, in the composite, the Nafion film, which is resistant to chemical corrosion, can effectively transport charges,[27] and the uniform and dense Cu-BDC film leads to an effective and stable HER. The described integration of the Cu-BDC film and Nafion film in composite has the potential to serve as a new-generation practical HER electrode, showcasing efficient hydrogen production capability. The wide range of applications of this electrode can be anticipated.

2. RESULTS AND DISCUSSION

Figure 1a illustrates the schematic demonstration of the fabrication process of the Cu-BDC@Nafion film, which is designed to achieve a high-performance electrocatalytic HER. The scanning electronic microscopy (SEM) image of the Nafion film is shown in Figure 1b. Subsequently, the ZnO nanomembrane with 300 consecutive ALD cycles (Figure S1) was deposited on the Nafion film (ZnO-Nafion film, Figure 1b). The thickness of the ZnO nanomembrane as an induction layer for the growth of Cu-BDC is ~50 nm. We noticed that a very thin ZnO nanomembrane can hardly induce the growth of Cu-BDC on the Nafion film, while a very thick ZnO nanomembrane with excessive ALD cycles is time-consuming, and the relatively large resistance of the nanomembrane may influence its electrochemical property. After this ALD pretreatment, no obvious morphology changes can be seen, indicating a uniform ZnO nanomembrane (Figure 1c). Then, the Cu-BDC film was conformally grown on the surface of the pretreated Nafion film via a solvothermal process (Figure 1d).[26] According to our previous research,[28] the growth mechanism and nucleation process of the Cu-BDC film under the induction of an ALD ZnO nanomembrane should be divided into a few steps.[28] First, the ZnO nanomembrane reacted with copper nitrate trihydrate to form (Zn, Cu) hydroxyl double salt (HDS). Subsequently, when exposed to the organic linker (H_2BDC), $COOH^-$ in H_2BDC provided reactive electrons to disrupt the crystal structure of HDS.[29] Consequently, in the third step, with gradual exposure to H_2BDC, Cu^{2+} was successively ligated with H_2BDC. Eventually, HDS was completely converted to Cu-BDC after the aging process. Owing to the conformal coating of the ALD ZnO nanomembrane, the Cu-BDC film on the Nafion film is uniform, dense, and firmly attached to the surface of the Nafion film. The composite demonstrates good HER ability at a suitable applied voltage, as will be discussed later (Figure 1a).

We further substantiated the structures of the samples by using X-ray diffraction (XRD), as depicted in Figure 2a. The extensive band observed at approximately $2\theta = 25°$ within the blank Nafion film is attributed to the amorphous nature of Nafion.[30] Upon depositing a ZnO nanomembrane (plot: ZnO-Nafion film), the XRD pattern shows sharp diffraction peaks, which correspond to polycrystalline wurtzite ZnO.[31] Subsequently, after Cu-BDC is assembled, the diffraction peaks (plot: Cu-BDC@Nafion film) align with those of Cu-BDC reported previously in literature.[32] Also, the Raman spectra of the Cu-BDC@Nafion film and the original Nafion film are shown in Figures S2 and S3, respectively, confirming the existence of BDC organic linkers.[26] In addition, thermal gravimetric analysis (TGA) of the Cu-BDC@Nafion film was performed to study the thermostability of the composite. In Figure 2b, when the temperature is higher than 350 °C, a gradual drop in mass can be observed due to the oxidation degradation of organic linkers.[33] This result proves the outstanding structural stability of the Cu-BDC@Nafion film in a wide temperature range. In addition, the TGA result indicates that the Cu-BDC content is 93.2% in the composite, which is beneficial for the HER process. Moreover, nitrogen adsorption−desorption isotherms were measured to investigate the pore structure of the composite (Figure 2c), and the

https://doi.org/10.1021/acsaem.4c00170
ACS Appl. Energy Mater. 2024, 7, 3406−3413

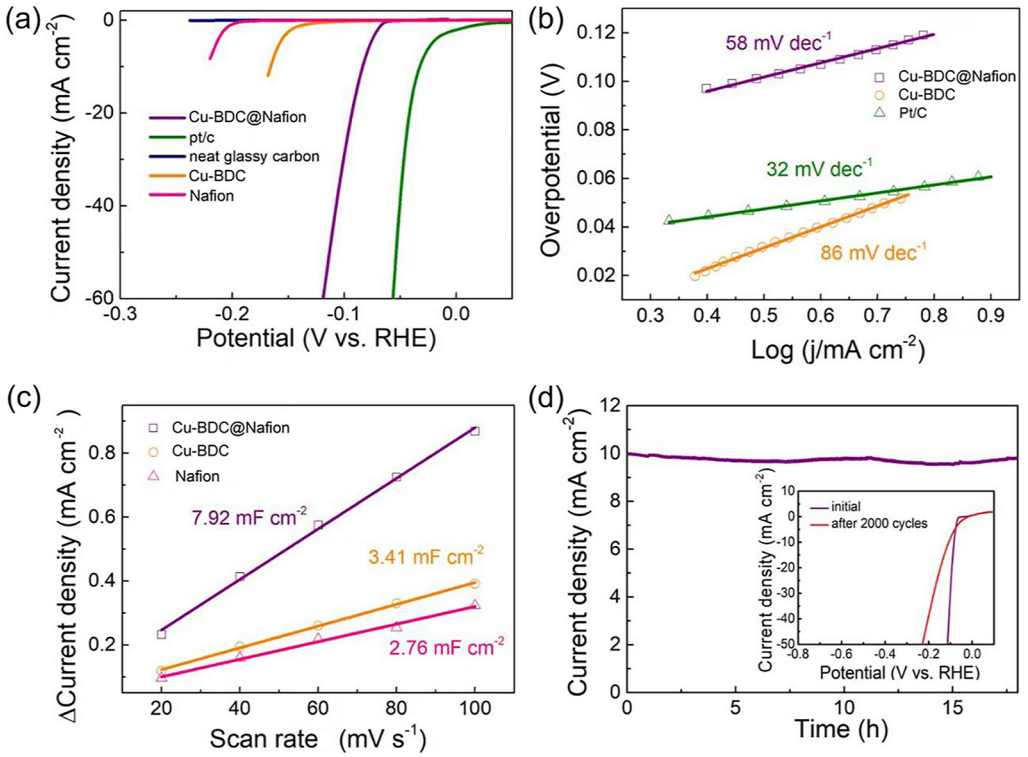

Figure 4. (a) LSV curves of the samples. (b) Tafel slopes of the samples. (c) Capacitance currents of the samples as a function of the scan rate. The slope of lines represents the corresponding C_{dl} values. (d) Chronopotentiometric durability test of the Cu-BDC@Nafion film at a constant current density of 10 mA cm^{-2} in 1.0 mM NaOH. The inset is the cycling stability measurement of the Cu-BDC@Nafion film before and after 2000 CV cycles.

calculated pore size distributions are shown in Figure 2d. Consistent with the isotherms, an open mesopore of 10 nm can be clearly observed in the Cu-BDC@Nafion film, and the surface area reaches 547 m^2 g^{-1}. The Nafion film demonstrates a very low specific surface area of 6 m^2 g^{-1}, and thus the porous structure can be neglected.

Furthermore, the elements' chemical states in the Cu-BDC@Nafion film were characterized by using X-ray photoelectron spectroscopy (XPS), affirming the presence of Cu, C, and O (Figure 3a). As displayed in Figure 3b, the high-resolution Cu 2p spectrum can be deconvoluted into seven peaks. Two characteristic peaks at 933.08 and 952.88 eV, along with their shoulder peaks at 934.58 and 954.48 eV, were ascribed to the Cu $2p_{3/2}$ and Cu $2p_{1/2}$ of Cu(I) and Cu(II), respectively.[34] The shakeup satellite peaks located at 939.68 and 943.88 eV and the other satellite peak at 962.28 eV further confirm the presence of Cu(II) species in the sample.[35] These may contribute to the high catalytic activity for high-performance HER applications as the evolution is mainly realized through the mutual conversion of Cu(I) and Cu(II).[36] Moreover, in Figure 3c, one can see three XPS peaks in the high-resolution C 1s XPS spectrum, which should originate from C═C/C−C (284.7 eV), C−O/C−H (285.5 eV), and O−C═O (288.5 eV) in Cu-BDC and the conductive Nafion substrate.[19] Three peaks of the O 1s spectrum at 531.38, 531.98, and 532.66 eV presented in Figure 3d are considered to be connected with the moieties of C═O, C−OH, and Cu−O, respectively.[37]

The combination of the conductive Nafion film and high-electrochemically active Cu ion renders the Cu-BDC@Nafion composite film promising in electrochemical applications like HER. According to the literature,[38] the HER of Cu-BDC might be described by the following reactions

$$\mathrm{Cu(II)-BDC} + \mathrm{H_2O} + \mathrm{e^-} \rightarrow \mathrm{Cu(I)-BDC} - \mathrm{H^*} + \mathrm{OH^-}$$

$$\mathrm{Cu(I)-BDC} - \mathrm{H^*} + \mathrm{H_2O} - \mathrm{e^-} \rightarrow \mathrm{Cu(II)-BDC} + \mathrm{OH^-} + \mathrm{H_2}$$

Here, the HER performance of the Cu-BDC@Nafion film electrode was experimentally investigated by using a typical three-electrode system. Generally, an efficient HER catalyst should exhibit low overpotential at a standard current density of 10 mA cm^{-2}, a low Tafel slope comparable to that of a Pt catalyst, and, meanwhile, remarkable cycling performance. Figure 4a illustrates the linear sweep voltammetry (LSV) results for Cu-BDC@Nafion as well as reference samples (Pt/C, neat glassy carbon, Cu-BDC, and blank Nafion film) in an aqueous electrolyte of 1.0 M NaOH at a scanning rate of 5 mV s^{-1}. Neat glassy carbon demonstrates no appreciable catalytic capacity, implying that all of the currents are connected with the tested samples. Conversely, the Pt/C-modified glassy carbon electrode used as a reference electrode has the lowest overpotential (i.e., excellent HER catalytic performance) at a current density of 10 mA cm^{-2}. Moreover, the horizontal lines at low potentials of the blank Nafion film indicate that it has almost no HER capability. Here, Cu-BDC powder shows apparent electrochemical activity due to the highly catalytic Cu ion, but the detected overpotential is ~166 mV vs RHE. The relatively low performance of the Cu-BDC powder may be attributed to the paucity of effective active sites on the

https://doi.org/10.1021/acsaem.4c00170
ACS Appl. Energy Mater. 2024, 7, 3406−3413

Table 1. Summary of HER Performances (in an Alkaline Electrolyte) of MOF-Based Structures and Nafion-Based Composites Reported in the Recent Literature

sample	electrolyte	overpotential (mV)	Tafel slope (mV dec−1)	stability	ref
Co@NC/NF	0.1 M KOH	240	126.8	50 h	40
$Co_{0.85}Se$@NC	1 M KOH	230	125	10 h	41
Co-NCF@600-Ni	1 M KOH	157	112	20 h and 3000 cycles	42
Co-N-CS-CF	1 M KOH	172	84	30 h	25
Fe-N-HLPCS	1 M KOH	70	55	20 h and 2000 cycles	43
Pt[NiFe]-Nafion	1 M NaOH	120	97	20 h	44
NiCu-Nafion	1 M KOH	200	120	30 h	45
Pd/Nafion	0.5 M NaOH	59	54	2000 cycles	46
Cu-BDC	1 M NaOH	166	86		this work
20% Pt/C	1 M NaOH	32	32		this work
Cu-BDC@Nafion	**1 M NaOH**	**84**	**58**	**18 h and 2000 cycles**	**this work**

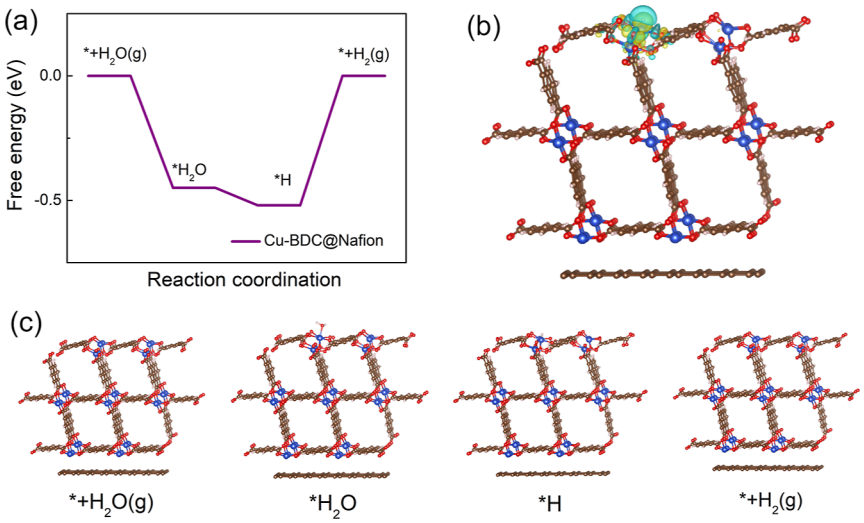

Figure 5. (a) Free energy diagram of the proposed reaction process. (b) Differential charge density of H_2O adsorbed on the Cu-BDC@Nafion film (side view). (c) DFT calculation models for each reaction step.

electrodes and the low electric conductivity. Furthermore, the dispersed rigid particles impede effective charge and ion transport, severely affecting the electrochemical properties.[39] Notably, the current density of the Cu-BDC@Nafion film reaches 10 mA cm^{-2} at only 84 mV (Figure 4a), demonstrating a much better HER performance. Further, the Tafel slopes of these samples are calculated based on the linear fitting of the polarization curves, and the results are illustrated in Figure 4b. The Tafel slope of the Cu-BDC@Nafion film is determined to be 58 mV dec^{-1}, which is significantly less than that of Cu-BDC (86 mV dec^{-1}). The hydrogen evolution of Cu-BDC@Nafion and the Cu-BDC electrode can be viewed as the Volmer step due to its low Tafel slope.[25] Here, we carried out cyclic voltammetry (CV) characterizations to measure electrochemical double-layer capacitance (C_{dl}) for determining the electrochemical surface area (ECSA) and active sites pertinent to electrocatalysis. The CV profiles for the samples at various scan rates varying from 20 mV to 100 mV s^{-1} are demonstrated in Figure S4, and corresponding linear fitting plots are shown in Figure 4c. The calculated results show that the Cu-BDC@Nafion film has a maximum C_{dl} of ∼7.92 mF cm^{-2}, compared to those of Cu-BDC powders (3.41 mF cm^{-2}) and Nafion film (2.76 mF cm^{-2}). This illustrates that the Cu-BDC@Nafion film has more exposed active sites and thus possesses excellent electrocatalytic properties toward HER. As a HER catalyst, the stability of continuous cycling is also crucial. Therefore, we conducted a chronopotentiometric durability test for the Cu-BDC@Nafion film. Figure 4d shows the result of a 16 h test, demonstrating significant stability. Then, we compare the initial LSV curve of the Cu-BDC@Nafion film with the curve obtained after 2000 CV cycles in the non-Faraday region. The LSV curves show a slight shift in current density and a small increase in the overpotential (inset of Figure 4d), which confirms the good long-term cycling stability of the Cu-BDC@Nafion film. Table 1 summarizes the HER performances of the composites prepared by the current strategy as well as similar MOF-based structures and Nafion-based composites reported in the literature, and one can see that the current Cu-BDC@Nafion film possesses excellent HER performance.

To gain a comprehensive perception of the electrochemical character of Cu-BDC@Nafion at the atomic level, density functional theory (DFT) calculations are executed to establish a mechanism of the enhanced HER performance perceived in this composite. These calculations adhered to the generalized gradient approximation within the Vienna ab initio simulation package (VASP). Referring to HER reactions, particular emphasis was placed on the H_2O dissociation−adsorption mechanism,[25] and the essential alkaline HER process is postulated to operate through the stages shown below

$$\text{Volmer step: } H_2O + 2e^- + {}^* \rightarrow H^* + OH^-$$

https://doi.org/10.1021/acsaem.4c00170
ACS Appl. Energy Mater. 2024, 7, 3406−3413

Tafel step: $H^* + H^* \rightarrow H_2$

Heyrovskystep: $H_2O + H^* + e^* \rightarrow H_2 + OH^- + *$

As illustrated in Figure 5a, the spontaneous progression of the reaction is signified by the gradual descent of the Gibbs free energy curve across the first two steps. Thus, it appears that the Heyrovsky step emerges as the critical phase of the overall reaction. Here, we divide the HER procedure under alkaline conditions into four distinct stages: initiation, catalytic hydrodissociation, hydrogen ion adsorption, and hydrogen generation. The calculated Gibbs free energy values related to hydrogen production are −0.52 ($*H_2O$) and −0.45 eV (H*), implying a reduced hydrogen affinity accompanied by a minimal energy barrier. The theoretical calculation, which reveals the kinetic reasons for the excellent alkaline HER activity of Cu-BDC@Nafion from a theoretical point of view, is consistent with the experimental results. For a more thorough understanding of the influence of charge transfer on catalytic capability, additional calculations were carried out by employing the free energy model, as demonstrated in Figure 5b. The top view of the charge transfer is displayed in Figure S5, together with a visualization of the entire reaction implementation in Figure 5c. The computational outcomes confirm that the integration of Cu ions establishes novel active sites, substantially reducing the HER overpotential, thereby expediting electron loss and optimizing the electrocatalytic function of the Cu-BDC@Nafion film.

3. CONCLUSIONS

In summary, a Cu-BDC@Nafion film composite has been fabricated by assembling Cu-BDC particles on a conductive Nafion film with the assistance of an ALD ZnO nanomembrane. The resultant composite exhibits a unique structure: a substantial amount of Cu-BDC crystals grow on the Nafion film to form a uniform and dense film, and the composite film with a hierarchically porous structure demonstrates a large surface area. The HER electrode prepared from the composite can function well in an alkaline electrolyte, and outstanding electrocatalytic performance such as an overpotential of 84 mV at 10 mA cm^{-2}, a Tafel slope of 58 mV dec^{-1}, and impressive stability (2000 cycles and 16 h without decline) in a 1.0 M NaOH electrolyte are observed. The results indicate that the integration of the Cu-BDC film on a conductive Nafion film makes the composite promising in HER. This investigation proclaims a viable methodology to fabricate MOF-based composites with prospects for both structural and method innovation as well as actionable applications in hydrogen generation.

4. EXPERIMENTAL SECTION

4.1. Materials. The Nafion film was procured from BASF Basotect (Shanghai, China). Copper nitrate trihydrate [$Cu(NO_3)_2{\cdot}3H_2O$], terephthalic acid (H_2BDC), and Nafion solution (5 wt %) were procured from Aladdin Ltd. (Shanghai, China). Ethanol (AR, ≥99.7%) was sourced from Titan Ltd. (Shanghai, China). Dimethyl formamide (AR, ≥99.5%) was procured from Sinopharm Chemicals. The Pt/C catalyst prepared by loading 20 wt % platinum on carbon black was provided by Alfa Aesar and used as a reference for comparative analysis. All the chemicals were utilized as supplied without subsequent purification. The DI water utilized throughout all experiments was purified using a Millipore system.

4.2. ZnO Nanomembrane Deposited by ALD. The deposition of the ZnO nanomembrane on the Nafion film was performed at 150 °C in a homemade reactor. Diethylzinc (DEZ) and DI water were used as the precursors. A typical ALD cycle included a DEZ pulse (50 ms), waiting time (5 s), N_2 purge (30 s), H_2O pulse (30 ms), waiting time (5 s), and N_2 purge (30 s). In the current study, a ZnO nanomembrane with 300 ALD cycles was deposited on a Nafion film.

4.3. Growth of the Cu-BDC Layer on Nafion. DMF (62 mL) and ethanol (4 mL) were mixed to form organic solvent A. $Cu(NO_3)_2{\cdot}3H_2O$ (1.93 g) was dissolved in organic solvent A to form solution B. H_2BDC (0.79 g) was dissolved in another organic solvent A to form solution C. Nafion films were then placed into a beaker containing solution B. The beaker was sealed at 90 °C for 24 h. After cooling to room temperature, solution C was added, and the mixture was aged at room temperature for another 24 h for the growth of the Cu-BDC film. After that, the composite film was taken out and washed with ethanol three times. The sample was subsequently dried in vacuum at 60 °C for 12 h.

4.4. Synthesis of the Cu-BDC Powder. Cu-BDC powder was concurrently synthesized for comparison. The solutions B and C were stirred vigorously for 5 min, followed by an aging process in a beaker at room temperature for 24 h. Afterward, the product was centrifuged, washed three times with ethanol, and finally dried under vacuum at 60 °C for 12 h.

4.5. Characterizations. The morphologies of all of the samples were measured by field-emission SEM (Phenom Prox). XRD patterns were achieved by an X'Pert Pro X-ray diffractometer equipped with Cu K_α radiation (λ = 0.1542 nm) at a current of 40 mA and a voltage of 40 kV. A Quadrasorb adsorption instrument (Quantachrome Instruments) was used to perform nitrogen sorption/desorption measurements. The specific surface area was calculated by using the multipoint Brunauer−Emmett−Teller (BET) method. The pore size distributions were calculated from nitrogen sorption data using the nonlocal DFT equilibrium model. XPS analyses were performed with VG ESCALAB 220I-XL equipment. The data analysis was accomplished with XPS Peak 4.1 software. TGA was measured via an STA8000 instrument with a 10 °C/min speed in an air environment. The electrochemical HER tests were evaluated on a CHI 660E electrochemical workstation (CH Instrument, Shanghai, China) with a three-electrode configuration and performed in different electrolytes. An Ag/AgCl electrode (in saturated KCl solution) was used as the reference electrode, and a graphite rod was used as the counter electrode. The working electrode was prepared by fixing the film sample on graphite paper with a 5% Nafion solution. For comparative purposes, Cu-BDC powder and Pt/C-modified glassy carbon (diameter: 3 mm) electrodes were also fabricated and characterized.

4.6. DFT Calculation. A first-principles computational analysis utilizing periodical DFT has been performed by employing the generalized gradient approximation within the Perdew−Burke−Ernzerhof exchange correction function. The wave functions were constructed from the expansion of plane waves with an energy cutoff of 450 eV and a gamma-centered k-point of 2 × 2 × 1. A consistence tolerance of 1.0×10^{-5} eV/atom for the total energy and 0.05 eV/Å for the applied forces has been stipulated. To minimize surface-to-surface interactions, a considerable separation of 15 Å was set between continuous layers in the periodically repeated slabs. In subsequent free energy computations, the entropic corrections and zero-point energy (ZPE) have been included. The free energy of species was calculated according to the standard formula

$$\Delta G = E + \Delta \mathrm{ZPE} + \Delta H - \Delta \mathrm{TS}$$

where ΔH is the integrated heat capacity, T is the temperature of the product, and S is the entropy.

■ ASSOCIATED CONTENT

Supporting Information

The Supporting Information is available free of charge at https://pubs.acs.org/doi/10.1021/acsaem.4c00170.

https://doi.org/10.1021/acsaem.4c00170
ACS Appl. Energy Mater. 2024, 7, 3406−3413

Detailed ALD process, Raman spectra of the samples, CV curves of the samples, and differential charge density of H_2O adsorbed on the Cu-BDC@Nafion film (PDF)

AUTHOR INFORMATION

Corresponding Authors

Zhe Zhao − *Department of Materials Science & State Key Laboratory of Molecular Engineering of Polymers, Fudan University, Shanghai 200438, P. R. China; College of Biological Science and Medical Engineering, Donghua University, Shanghai 201620, P. R. China*; Email: zhezhao@dhu.edu.cn

Gaoshan Huang − *Department of Materials Science & State Key Laboratory of Molecular Engineering of Polymers, Fudan University, Shanghai 200438, P. R. China; Yiwu Research Institute of Fudan University, Yiwu 322000 Zhejiang, P. R. China; International Institute for Intelligent Nanorobots and Nanosystems, Fudan University, Shanghai 200438, P. R. China*; orcid.org/0000-0002-0525-7177; Email: gshuang@fudan.edu.cn

Authors

Zhijia Xiao − *Department of Materials Science & State Key Laboratory of Molecular Engineering of Polymers, Fudan University, Shanghai 200438, P. R. China; Yiwu Research Institute of Fudan University, Yiwu 322000 Zhejiang, P. R. China; International Institute for Intelligent Nanorobots and Nanosystems, Fudan University, Shanghai 200438, P. R. China*

Jinlong Wang − *Department of Materials Science & State Key Laboratory of Molecular Engineering of Polymers, Fudan University, Shanghai 200438, P. R. China; Yiwu Research Institute of Fudan University, Yiwu 322000 Zhejiang, P. R. China; International Institute for Intelligent Nanorobots and Nanosystems, Fudan University, Shanghai 200438, P. R. China*; orcid.org/0000-0002-1444-0838

Xinyi Ke − *Department of Materials Science & State Key Laboratory of Molecular Engineering of Polymers, Fudan University, Shanghai 200438, P. R. China; Yiwu Research Institute of Fudan University, Yiwu 322000 Zhejiang, P. R. China; International Institute for Intelligent Nanorobots and Nanosystems, Fudan University, Shanghai 200438, P. R. China*

Zihan Lu − *Department of Materials Science & State Key Laboratory of Molecular Engineering of Polymers, Fudan University, Shanghai 200438, P. R. China; Yiwu Research Institute of Fudan University, Yiwu 322000 Zhejiang, P. R. China; International Institute for Intelligent Nanorobots and Nanosystems, Fudan University, Shanghai 200438, P. R. China*

Yongfeng Mei − *Department of Materials Science & State Key Laboratory of Molecular Engineering of Polymers, Fudan University, Shanghai 200438, P. R. China; Yiwu Research Institute of Fudan University, Yiwu 322000 Zhejiang, P. R. China; International Institute for Intelligent Nanorobots and Nanosystems, Fudan University, Shanghai 200438, P. R. China*; orcid.org/0000-0002-3314-6108

Complete contact information is available at: https://pubs.acs.org/10.1021/acsaem.4c00170

Author Contributions

Z.X. and J.W. contributed equally to this work.

Notes

The authors declare no competing financial interest.

ACKNOWLEDGMENTS

This work is supported by the National Key Technologies R&D Program of China (no. 2021YFA0715302), the National Natural Science Foundation of China (no. 52203328), and the Science and Technology Commission of Shanghai Municipality (nos. 22ZR1405000 and 21142200200).

REFERENCES

(1) Pratama, D. S. A.; Haryanto, A.; Lee, C. W. Heterostructured mixed metal oxide electrocatalyst for the hydrogen evolution reaction. *Front. Chem.* **2023**, *11*, 1141361.

(2) Abdin, Z.; Al Khafaf, N.; McGrath, B.; Catchpole, K.; Gray, E. A review of renewable hydrogen hybrid energy systems towards a sustainable energy value chain. *Sustainable Energy Fuels* **2023**, *7* (9), 2042−2062.

(3) Sarker, A. K.; Azad, A.; Rasul, M. G.; Doppalapudi, A. T. Prospect of green hydrogen generation from hybrid renewable energy sources: a review. *Energies* **2023**, *16*, 1556.

(4) Dai, F.; Zhang, S. P.; Luo, Y. P.; Wang, K.; Liu, Y. R.; Ji, X. Y. Recent progress on hydrogen-rich syngas production from coal gasification. *Processes* **2023**, *11*, 1765.

(5) Chen, W. H.; Biswas, P. P.; Ubando, A. T.; Park, Y. K.; Ashokkumar, V.; Chang, J. S. Design of experiment for hydrogen production from ethanol reforming: A state-of-the-art review. *Fuel* **2023**, *342*, 127871.

(6) Wang, C. P.; Lin, Y. X.; Cui, L.; Zhu, J.; Bu, X. H. 2D Metal-organic frameworks as competent electrocatalysts for water splitting. *Small* **2023**, *19*, 207342.

(7) Chen, Z. L.; Qing, H. L.; Zhou, K.; Sun, D. L.; Wu, R. B. Metal-organic framework-derived nanocomposites for electrocatalytic hydrogen evolution reaction. *Prog. Mater. Sci.* **2020**, *108*, 100618.

(8) Zhou, F.; Zhou, Y.; Liu, G. G.; Wang, C. T.; Wang, J. Recent advances in nanostructured electrocatalysts for hydrogen evolution reaction. *Rare Met.* **2021**, *40*, 3375−3405.

(9) Radwan, A.; Jin, H. H.; He, D. P.; Mu, S. C. Design engineering, synthesis protocols, and energy applications of MOF-derived electrocatalysts. *Nano-Micro Lett.* **2021**, *13*, 132.

(10) Ma, W.; Zhang, X. Y.; Li, W. Y.; Jiao, M. G.; Zhang, L. L.; Ma, R. Z.; Zhou, Z. Advanced Pt-based electrocatalysts for the hydrogen evolution reaction in alkaline medium. *Nanoscale* **2023**, *15*, 11759−11776.

(11) Guo, F.; Macdonald, T. J.; Sobrido, A. J.; Liu, L. X.; Feng, J. R.; He, G. J. Recent advances in ultralow-Pt-loading electrocatalysts for the efficient hydrogen evolution. *Adv. Sci.* **2023**, *10*, 2301098.

(12) Miao, M.; Pan, J.; He, T.; Yan, Y.; Xia, B. Y.; Wang, X. Molybdenum carbide-based electrocatalysts for hydrogen evolution reaction. *Chem. Eur. J.* **2017**, *23*, 10947−10961.

(13) Wan, P. F.; Tang, Q. Theoretical progress of MXenes as electrocatalysts for the hydrogen evolution reaction. *Mater. Chem. Front.* **2024**, *8*, 507−527.

(14) Qin, X. P.; Ola, O.; Zhao, J. Y.; Yang, Z. H.; Tiwari, S. K.; Wang, N. N.; Zhu, Y. Q. Recent progress in graphene-based electrocatalysts for hydrogen evolution reaction. *Nanomaterials* **2022**, *12* (11), 1806.

(15) Zhong, L.; Qian, J. J.; Wang, N.; Komarneni, S.; Hu, W. C. Metal-organic frameworks on versatile substrates. *J. Mater. Chem. A* **2023**, *11*, 20423−20458.

(16) Zuliani, A.; Khiar, N.; Carrillo-Carrion, C. Recent progress of metal-organic frameworks as sensors in (bio)analytical fields: towards real-world applications. *Anal. Bioanal. Chem.* **2023**, *415* (11), 2005−2023.

(17) Zhou, Z. C.; Xu, L. N.; Ding, Y. H.; Xiao, H. P.; Shi, Q.; Li, X. H.; Li, A. D.; Fang, G. Y. Atomic layer deposition meets metal-organic frameworks. *Prog. Mater. Sci.* **2023**, *138*, 101159.

(18) Lin, J. P.; Wu, Q. L.; Qiao, J.; Zheng, S. A.; Liu, W.; Wu, L. L.; Liu, J. R.; Zeng, Z. H. A review on composite strategy of MOF derivatives for improving electromagnetic wave absorption. *iScience* **2023**, *26* (7), 107132.
(19) Habibi, N.; Faraji, S.; Pourjavadi, A. Nano graphite platelets/Cu (BDC) MOF coating on polyurethane sponge: A superhydrophobic self-extinguishing adsorbent for static and continuous oil/water separation. *Colloids Surf., A* **2023**, *676*, 132186.
(20) Abdollahi, B.; Farshnama, S.; Abbasi Asl, E.; Najafidoust, A.; Sarani, M. Cu(BDC) metal-organic framework (MOF)-based Ag_2CrO_4 heterostructure with enhanced solar-light degradation of organic dyes. *Inorg. Chem. Commun.* **2022**, *138*, 109236.
(21) Zhou, Y. J.; Chen, Y. K.; Liu, L.; Zhao, Q.; Jiang, T. S. Design and preparation of three-dimensional core-shell structures CF@Cu-BDC@NiCo-LDH for high-performance battery-type supercapacitors and oxygen evolution reaction. *J. Taiwan Inst. Chem. Eng.* **2023**, *144*, 104643.
(22) Tang, J.; Shen, Y.; Miao, X.; Qin, H.; Song, D.; Li, Y.; Qu, Y.; Yin, Z.; Ren, J.; Wang, L.; Wang, B. Template-directed growth of hierarchically structured MOF-derived LDH cage hybrid arrays for supercapacitor electrode. *J. Electroanal. Chem.* **2019**, *840*, 174−181.
(23) Xu, Y.; Yu, S. S.; Ren, T. L.; Liu, S. L.; Wang, Z. Q.; Li, X. N.; Wang, L.; Wang, H. J. Hydrophilic/aerophobic hydrogen-evolving electrode: NiRu-based metal-organic framework nanosheets in situ grown on conductive substrates. *ACS Appl. Mater. Interfaces* **2020**, *12* (31), 34728−34735.
(24) Li, H. Y.; Zhao, S. N.; Zang, S. Q.; Li, J. Functional metal-organic frameworks as effective sensors of gases and volatile compounds. *Chem. Soc. Rev.* **2020**, *49*, 6364−6401.
(25) Zhao, Z.; Zhang, Z.; Zhao, Y.; Liu, J.; Liu, C.; Wang, Z.; Zheng, G.; Huang, G.; Mei, Y. Atomic layer deposition inducing integration of Co, N codoped carbon sphere on 3D foam with hierarchically porous structures for flexible hydrogen producing device. *Adv. Funct. Mater.* **2019**, *29*, 1906365.
(26) Zhao, Z.; Kong, Y.; Huang, G.; Liu, C.; You, C.; Xiao, Z.; Zhu, H.; Tan, J.; Xu, B.; Cui, J.; Liu, X.; Mei, Y. Area-selective and precise assembly of metal organic framework particles by atomic layer deposition induction and its application for ultra-sensitive dopamine sensor. *Nano Today* **2022**, *42*, 101347.
(27) Wang, Q. C.; Shen, D. C.; Tu, Z. K.; Li, S. Improved performance of lanthanide-doped UIO-66/Nafion hybrid proton exchange membrane for water electrolyzer. *Int. J. Hydrogen Energy* **2024**, *56*, 1249−1256.
(28) Zhao, Z.; Kong, Y.; Lin, X. Y.; Liu, C.; Liu, J. R.; He, Y. Y.; Yang, L. L.; Huang, G. S.; Mei, Y. F. Oxide nanomembrane induced assembly of a functional smart fiber composite with nanoporosity for an ultra-sensitive flexible glucose sensor. *J. Mater. Chem. A* **2020**, *8*, 26119−26129.
(29) Ma, C. C.; Gao, G. S.; Liu, H. O.; Liu, Y.; Zhang, X. F. Fabrication of 2D bimetallic metal-organic framework ultrathin membranes by vapor phase transformation of hydroxy double salts. *J. Membr. Sci.* **2022**, *644*, 120167.
(30) Chen, T.; Lv, B.; Sun, S.; Hao, J.; Shao, Z. Novel Nafion/Graphitic Carbon Nitride Nanosheets Composite Membrane for Steam Electrolysis at 110 °C. *Membranes* **2023**, *13*, 308.
(31) Rahmah, M. I.; Qasim, H. B. A novel method to prepare antibacterial ZnO nanoflowers. *Appl. Phys. A: Mater. Sci. Process.* **2022**, *128*, 998.
(32) Taheri, S.; Mollabagher, H.; Seyed Mousavi, S. A. H. Metal organic framework Cu-BDC as an efficient and reusable catalyst for one-pot synthesis of benzophenazine derivatives. *Polycyclic Aromat. Compd.* **2022**, *42*, 6523−6536.
(33) Nayak, A.; Viegas, S.; Dasari, H.; Sundarabal, N. Cu-BDC and Cu_2O derived from Cu-BDC for the removal and oxidation of asphaltenes: a comparative study. *ACS Omega* **2022**, *7*, 34966−34973.
(34) Huang, Y. L.; Fan, X. T.; Zhou, Y. P.; Liu, S. R.; Li, Y. Q. In situ growth of Cu(BDC) on microscale Cu-based carboxymethylcellulose fibers: A new strategy for constructing efficient catalysts for A^3-coupling reactions. *Appl. Organomet. Chem.* **2023**, *37*, No. e7041.
(35) Al-Thabaiti, S. A.; Mostafa, M. M. M.; Ahmed, A. I.; Salama, R. S. Synthesis of copper/chromium metal organic frameworks-Derivatives as an advanced electrode material for high-performance supercapacitors. *Ceram. Int.* **2023**, *49*, 5119−5129.
(36) Ahmed, A.; Robertson, C. M.; Steiner, A.; Whittles, T.; Ho, A.; Dhanak, V.; Zhang, H. Cu(I)Cu(II)BTC, a microporous mixed-valence MOF via reduction of HKUST-1. *RSC Adv.* **2016**, *6*, 8902−8905.
(37) Gupta, N. K.; Kim, S.; Bae, J.; Soo Kim, K. Fabrication of $Cu(BDC)_{0.5}$ $(BDC\text{-}NH_2)_{0.5}$ metal-organic framework for superior H_2S removal at room temperature. *Chem. Eng. J.* **2021**, *411*, 128536.
(38) Rong, J.; Qiu, F. X.; Zhang, T.; Fang, Y. Y.; Xu, J. C.; Zhu, Y. Self-directed hierarchical Cu_3(PO4)2/Cu-BDC nanosheets array based on copper foam as an efficient and durable electrocatalyst for overall water splitting. *Electrochim. Acta* **2019**, *313*, 179−188.
(39) Ouyang, H.; Jiang, D.; Fan, Y.; Wang, Z. L.; Li, Z. Self-powered technology for next-generation biosensor. *Sci. Bull.* **2021**, *66*, 1709−1712.
(40) Aijaz, A.; Masa, J.; Rösler, C.; Xia, W.; Weide, P.; Fischer, R. A.; Schuhmann, W.; Muhler, M. Metal-organic framework derived carbon nanotube grafted cobalt/carbon polyhedra grown on nickel foam: an efficient 3D electrode for full water splitting. *Chemelectrochem* **2017**, *4*, 188−193.
(41) Meng, T.; Qin, J.; Wang, S.; Zhao, D.; Mao, B.; Cao, M. In situ coupling of $Co_{0.85}Se$ and N-doped carbon via one-step selenization of metal-organic frameworks as a trifunctional catalyst for overall water splitting and Zn-air batteries. *J. Mater. Chem. A* **2017**, *5*, 7001−7014.
(42) Zhang, Z.; Deng, L.; Zhao, Z.; Zhao, Y.; Yang, J.; Jiang, J.; Huang, G.; Mei, Y. Nickel nanograins anchored on a carbon framework for an efficient hydrogen evolution electrocatalyst and a flexible electrode. *J. Mater. Chem. A* **2020**, *8*, 3499−3508.
(43) Wang, Y.; Jin, L.; Hua, S.; Zhao, Z.; Xiao, Z.; Qu, C.; Huang, J.; Huang, G.; Ke, X.; Lu, Z.; Tan, J.; Liu, X.; Mei, Y. Hierarchically nanostructured nitrogen-doped porous carbon multi-layer confining Fe particles for high performance hydrogen evolution. *J. Mater.* **2023**, *9*, 1113−1121.
(44) Giesbrecht, P. K.; Müller, A. M.; Read, C. G.; Holdcroft, S.; Lewis, N. S.; Freund, M. S. Vapor-fed electrolysis of water using earth-abundant catalysts in Nafion or in bipolar Nafion/poly-(benzimidazolium) membranes. *Sustainable Energy Fuels* **2019**, *3*, 3611−3626.
(45) Faid, A. Y.; Barnett, A. O.; Seland, F.; Sunde, S. NiCu mixed metal oxide catalyst for alkaline hydrogen evolution in anion exchange membrane water electrolysis. *Electrochim. Acta* **2021**, *371*, 137837.
(46) Qu, Y. N.; Wen, S. Y.; Chen, J. H.; Shen, H. H.; Yu, W. J.; Wei, D.; Yu, J. G.; Kwon, Y. U.; Zhao, Y. N. Nafion-assisted synthesis of palladium nanonetworks as efficient electrocatalysts for hydrogen evolution reaction. *Ionics* **2020**, *26*, 1347−1356.

https://doi.org/10.1021/acsaem.4c00170
ACS Appl. Energy Mater. 2024, 7, 3406−3413